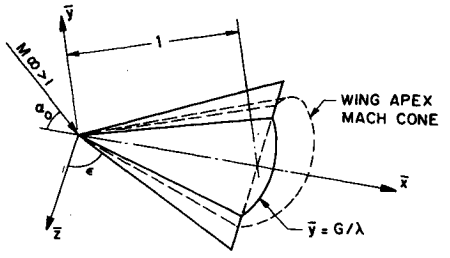


**Fig. 1 Configuration showing notation.**

mentioned above in Malmuth's paper can indeed be removed, and the area rule governing the total force applies for both hypersonic and supersonic flow with attached shock wave past delta wing with the addition on its compression side of a conical body of arbitrary shape.

Consider the flow over the compression side of a delta wing-body configuration at an incidence to a hypersonic or supersonic freestream (see Fig. 1). The same notation as Ref. 3 will be used and the combination of the freestream Mach number, the angle of incidence and the sweep-back angle is assumed to be such that the bow shock is attached to the leading edges. In the outer regions near the leading edges the flow is uniform and conically supersonic, and can be calculated exactly. On the other hand, in the inner region, which borders the outer regions at the wing apex Mach cone, the flow is nonuniform and conically subsonic, and is difficult to calculate exactly. However, it is shown in Ref. 3 that the flow in the inner region differs only slightly from the corresponding two-dimensional flow past a flat plate obtained by reducing the sweep angle to zero. This flat plate flow will be called reference flow and referred to with a subscript $o$. Thus $u_o$, $p_o$, $\rho_o$ and $M_o$ are, respectively, the velocity, pressure, density and Mach number of the reference flow.

Let $\delta$ be a small parameter characterizing the departure of the real flow in the inner region from the reference flow, and write the physical quantities as

$$\bar{u} = u_o(1+u), \quad \bar{v} = u_o v, \quad \bar{w} = u_o w$$
$$\bar{p} = p_o[1+(\gamma M_o^2/\lambda)p], \quad \bar{\rho} = \rho_o[1+(M_o^2/\lambda)\rho] \qquad (1)$$
$$\lambda = (M_o^2-1)^{1/2}$$

then $u = 0(\delta)$, etc. Conical coordinates $\eta$ and $\zeta$ are introduced as below

$$\eta = \lambda\bar{y}/\bar{x}, \quad \zeta = \lambda\bar{z}/\bar{x} \qquad (2)$$

Let the equation of the additional symmetrical conical body on the compression side be

$$\eta = G(\zeta) \qquad (3)$$

and assume that $G$ and $dG/d\zeta$ are $0(\delta)$. Furthermore, the addition of the conical body is limited to the wing apex Mach cone in the reference flow, i.e., $G = 0$ for $|\zeta| \geqq 1$. Under these conditions, the addition of the conical body will not affect the flow in the outer regions, and also the flow in the inner region will still differ from the reference flow by $0(\delta)$.

When terms $0(\delta^2)$ are neglected, the mixed boundary value problem for the perturbation pressure $p$ in the inner region is[3]

$$(\eta^2-1)\frac{\partial^2 p}{\partial\eta^2} + 2\eta\zeta\frac{\partial^2 p}{\partial\eta\,\partial\zeta} + (\zeta^2-1)\frac{\partial^2 p}{\partial\zeta^2} + 2\eta\frac{\partial p}{\partial\eta} + 2\zeta\frac{\partial p}{\partial\zeta} = 0 \qquad (4a)$$

$$p = 0, \quad \text{at} \quad \eta^2+\zeta^2 = 1 \qquad (4b)$$

$$\frac{\partial p}{\partial\zeta} = 0, \quad \text{at} \quad \zeta = 0 \qquad (4c)$$

$$\frac{\partial p}{\partial\eta} = -\frac{\zeta^2}{\lambda}G''(\zeta), \quad \text{at} \quad \eta = 0 \qquad (4d)$$

$$\frac{\partial p}{\partial\eta} + \left[-\frac{A_o+H}{1-H^2}\zeta + \frac{HB_o}{(1-H^2)\zeta}\right]\frac{\partial p}{\partial\zeta} = 0, \quad \text{at} \quad \eta = H \qquad (4e)$$

$$\int_o^{(1-H^2)^{1/2}} \frac{dp}{\zeta} = w^*/B_o, \quad \text{at} \quad \eta = H \qquad (4f)$$

where $A_o$, $B_o$, $H$ and $w^*$ are constants given in Ref. 3 [see, respectively, Eqs. (22, 16 and 5)].

This problem is in exactly the same form as that of Ref. 2. Defining the spanwise integral of pressure by

$$P \equiv \int_o^{(1-\eta^2)^{1/2}} p\,d\zeta \qquad (5)$$

we have,

$$P''(\eta) = 0, \qquad P'(0) = -V/\lambda$$
$$P'(H) + [(A_0+H)/(1-H^2)]P(H) = -Hw^*/(1-H^2) \qquad (6)$$

The solution of (6) is

$$P = -(V/\lambda)\eta + [V(1+A_o H)/\lambda(A_o+H)] - w^*H/(A_o+H) \qquad (7)$$

where

$$V = 2\int_o^1 G(\zeta)\,d\zeta \qquad (8)$$

is proportional to the volume of the additional body.

With the spanwise integral of pressure given by Eq. (5), the total pressure force $\vec{F}$ on the wing-body is found as follows†

$$\vec{F} = \frac{p_o}{\lambda^2}\left[\vec{i}\,V - \vec{j}\left\{\lambda + \frac{\gamma M_o^2}{A_o+H}(V+A_o HV-w^*H)\right\}\right] + \vec{F}_1 \qquad (9)$$

where $\vec{i}$ and $\vec{j}$ are, respectively, the unit vectors in $\bar{x}$ and $\bar{y}$ direction, and $\vec{F}_1$ represents the force contribution from the outer regions of the compression surface, and from the expansion surface (this may not be negligible for moderate supersonic flow) of the wing-body configuration. Since $\vec{F}_1$ is not affected by the addition of the conical body within the wing apex Mach cone, we conclude from Eq. (9) that the total pressure force on a delta wing-body configuration with attached shock wave in hypersonic or supersonic flow depends linearly on the volume of the additional conical body, and is independent of its cross-sectional shape. This constitutes the extension of Malmuth's hypersonic area rule.

## References

[1] Ladyzhenskii, M. D., "Hypersonic Area Rule," *AIAA Journal*, Vol. 1, No. 11, Nov. 1963, pp. 2696–2698.

[2] Malmuth, N., "A New Area Rule for Hypersonic Wing-Bodies," *AIAA Journal*, Vol. 9, No. 12, Dec. 1971, pp. 2460–2462.

[3] Hui, W. H., "Supersonic and Hypersonic Flow with Attached Shock Waves over Delta Wings," *Proceedings of the Royal Society of London*, Ser. A, Vol. 325, 1971, pp. 251–268.

† The base pressure is neglected in this analysis.

# Laser Velocimeter Measurement of Reynolds Stress and Turbulence in Dilute Polymer Solutions

SAMUEL E. LOGAN*
*California Institute of Technology, Pasadena, Calif.*

Received January 24, 1972.
Index category: Boundary Layers and Convective Heat Transfer—Turbulent.

* Graduate Student, Aeronautics. Fannie and John Hertz Foundation Fellow. Student Member AIAA.

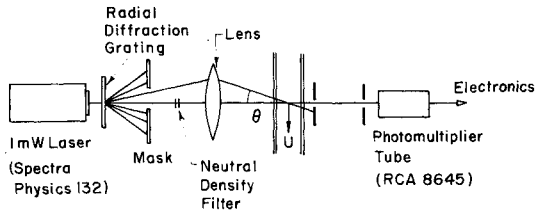


**Fig. 1 Optical geometry.**

### Introduction

SINCE 1948 when the Tom's effect of drag reduction was discovered[1] much experimental and theoretical work has been carried out on dilute drag reducing aqueous polymer solutions. Although the subject is still far from completely understood, recent results[2,3] have seemingly confirmed that a thickened viscous sublayer near the wall is consistent with the observed turbulent drag reduction. The most definitive measurements of velocity profile and axial turbulence intensity near the wall appear to have been made by Rudd[3] in a $\frac{1}{2}$-in.-sq pipe flow using a laser velocimeter. However, no information was given by these experiments on the effect of polymer additives on the transverse components of turbulence or the Reynolds stress. A laser velocimeter technique has been developed in the von Kármán Laboratory of Fluid Mechanics which is capable of measuring not only mean velocity $\langle u \rangle$ and axial turbulence intensity $\langle u'^2 \rangle^{1/2}$ but also transverse fluctuations $\langle v'^2 \rangle^{1/2}$ and the Reynolds stress $\langle u'v' \rangle$.[4] Work in progress on dilute aqueous polymer solutions indicates general agreement with Rudd's measurements of $\langle u \rangle$ and $\langle u'^2 \rangle^{1/2}$ in magnitude and behavior. In addition, measurements of $\langle u'v' \rangle$ and $\langle v'^2 \rangle$ indicate general reductions near the wall and outside the sublayer for polymer solutions relative to water.

### Apparatus

A square pipe of side $2R = \frac{1}{2}$ in. and $l/d = 70$ was selected for ease of making laser measurements near the wall. A constant-head tank is used as a supply which is filled by a pump for water measurements and manually by bucket for polymer to minimize degradation effects.

The optical system employed is described in detail in an earlier Note[4] and is designed to allow measurement of turbulence fluctuations in both the axial and transverse directions as well as the Reynolds stress correlation with only minor adjustments in optical geometry. Figure 1 diagrams the major optical components. A radial diffraction grating is employed as a combined beam splitter, measurement direction selector and frequency shifter. Self-alignment is assured through focus by a single lens and use of the undeflected laser beam as the reference beam passing through fixed apertures. The optics remain stationary and the tube is traversed by means of a micrometer with resolution of 0.001 in.

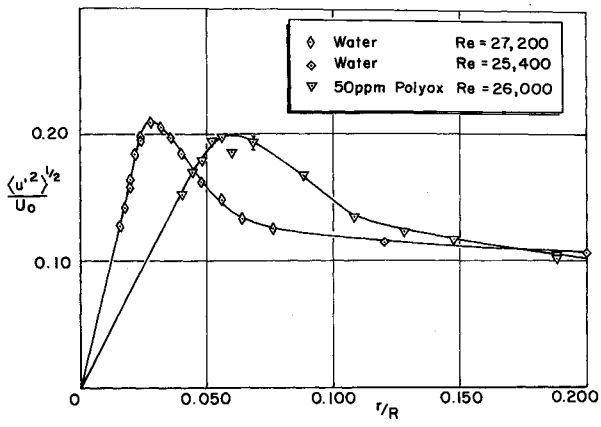


**Fig. 3 Axial intensity near the wall.**

### Results

Turbulence levels, $\langle u'^2 \rangle^{1/2}/U_o$, etc. measured in the square pipe are slightly higher than similar results obtained by Laufer and others for round tubes but are consistant in magnitude with Rudd's laser velocimeter measurements in a similar square pipe when normalized with $u_\tau$. It is possible that the existence o secondary flows in the square tube contribute to the slightly higher turbulence levels, although the secondary (radial) velocities actually measured have been small in magnitude, less than 0.5% of the centerline velocity. In any case, comparison between water and polymer flow at identical Reynolds number should yield valid trends in relative turbulence parameters.

Figure 2 presents measurements of axial and transverse turbulent fluctuations for water and 50 ppm polyox solution Most evident are the thickened sublayer for the polymer solution as evidenced by the displaced maximum of $\langle u'^2 \rangle^{1/2}$ as detailed in Fig. 3 and the markedly reduced slope of $\langle v'^2 \rangle^{1/2}$ which is more clearly seen in the normalized plot of Fig. 4. This result appears to indicate that polymer additives suppress transverse velocity fluctuations to a distance considerably beyond the viscous sublayer, although the magnitudes in the tube center are of comparable magnitude.

Figure 5 compares the measured Reynolds stress for water and polymer solution. It is observed that $\langle u'v' \rangle$ is reduced in the turbulent core by an amount proportional to the observed decrease in pressure gradient (or shear stress) at the wall. A comparison can be made between the least squares fit for the polymer (between $r/R = 0.125$ and 1.000) and an "expected

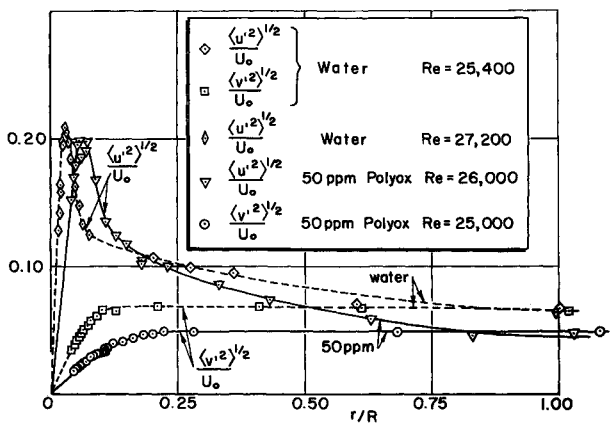


**Fig. 2 Axial and transverse turbulence intensities across the pipe.**

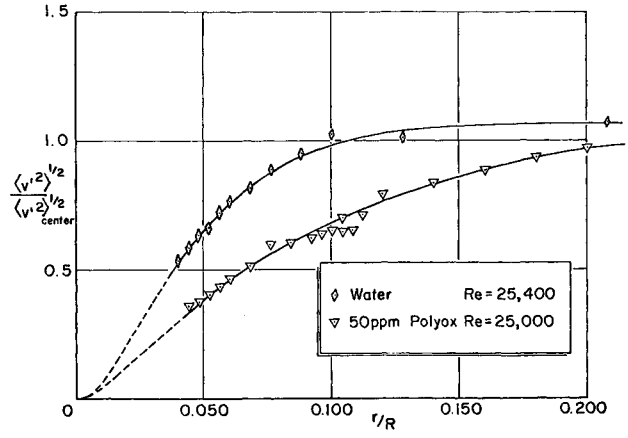


**Fig. 4 Normalized transverse turbulence intensity near the wall.**

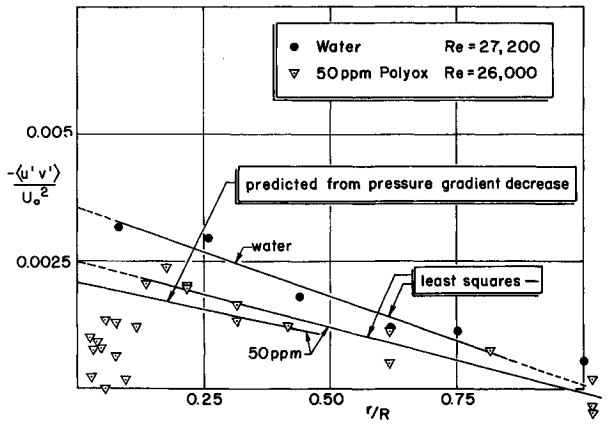


**Fig. 5 Reynolds stress across the pipe.**

extrapolated line based on the observed pressure drop at the wall, relative to the observed pressure drop for water.

Of considerable interest is the marked reduction of $\langle u'v'\rangle$ for the polymer solution in the region $0 < r/R < 0.125$. This seems to indicate that $u'$ and $v'$ are very greatly out of phase to a distance of approximately twice that of the $\langle u'^2\rangle^{1/2}$ peak. It is hoped that future explanations of these and subsequent measurements will help provide a basis for increased understanding of the mechanism of drag reduction by polymer additives.

### References

[1] Toms, B. A., "Some Observations on the Flow of Linear Polymer Solutions Through Straight Tubes at Large Reynolds Numbers," *Proceedings of First International Rheological Congress*, Holland, 1948, pp. 135–141.

[2] Virk, P. S. et al., "The Toms Phenomenon: Turbulent Pipe Flow of Dilute Polymer Solutions," *Journal of Fluid Mechanics*, Vol. 30, Pt. 2, Nov. 1967, pp. 305–328.

[3] Rudd, M. J., "Measurements Made on a Drag Reducing Solution With a Laser Velocimeter," *Nature*, Vol. 224, Nov. 1969, pp. 587–588.

[4] Logan, S. E., "A Laser Velocimeter for Reynolds Stress and Other Turbulence Measurements," *AIAA Journal*, to be published.

# Rational Reduction of Large-Scale Eigenvalue Problems

KARI APPA,* G. C. C. SMITH,† AND J. T. HUGHES‡
*Bell Aerospace Company/Division of Textron Inc., Buffalo, N.Y.*

### Introduction

EIGENVALUE analysis of the large dynamic matrices associated with complex structures can be computationally costly and unwieldy. Usually some form of "condensation" is carried out to reduce the matrix sizes involved[1,2] and the cost of determining the modest number of eigenvalues generally required. The most appropriate freedoms to be condensed from the total can be partly determined by judgement (e.g., rotational freedoms in a beam element), but in a "compact," complex structure it is difficult to decide on a completely rational and adequate division of retained and condensed freedoms.

There is, therefore, a need for a rational, scientific approach to the determination of the optimum set of freedoms to retain, which merely leaves the analyst to specify the number of freedoms to be retained. Such a procedure must justify itself economically in the total problem of arriving at the required information.

In Ref. 3, Lanczos' iteration procedure[4] was used to reduce a large system to a reduced rank tridiagonal form. Although improved numerical stability was thereby achieved, the selection of transformation vectors satisfying orthogonality conditions required considerable computational effort.

In this Note, transformation vectors are selected from coordinates which determine the largest (approximate) "swept volume" (area times deformation) generated by the local inertia force per unit acceleration. These are termed "maximum volume" modes, and, with attention to independency, form the basis for the rational choice of freedoms to be retained or condensed.

The deformation modes and their selection involve small computational effort typical only of "static" solutions. Basic principles for supported and free-free structures are outlined and a few simple examples illustrated.

### Approach

Any eigenfunction can be approximated as a linear combination of "static" deformation modes. To extract the most significant freedoms for the determination of a subset of lowest eigenvalues weighted consideration of both inertial and flexibility characteristics is required.

Let

$$Kq = -M\ddot{q} \tag{1}$$

where

$K = n \times n$ symmetric stiffness matrix
$M = n \times n$ symmetric inertia matrix
} of the complete structural model

and let $K$ be resolved into upper and lower triangular matrices $L$, $U$, i.e., such that

$$K = LU \tag{2}$$

and let $M_p$ = a rectangular $(n \times p)$ mass matrix with respect to potentially "significant" inertia loads, i.e., excluding those obviously ripe for condensation.

$M_p$ may range from the complete inertia matrix down to the consideration of nonstructural inertias (including contained fluids) only.

Assuming in turn $\ddot{q}_p = 1$, a set of deformation vectors can be generated by the usual static analysis routine (again using $L$, $U$) which may be written

$$[D]_p = [LU]^{-1}[M]_p \tag{3}$$

Maximum volume deformation modes are now determined by ranking the norms of the vectors of $[D]_p$, i.e.,

$$Q_i = \left(\sum_j D_{ij}^2\right)^{1/2} \quad \text{for} \quad i,j = 1 \ldots p \tag{4}$$

Let "$r$" ($\ll n, p$) be the rough number of deformation modes required to determine "$s$" eigenvalues. Then a good choice of columns appears to be the "$r$" largest of the $Q_i$'s.

The fundamental success of the method will be judged by the smallness of the ratio $(r/s)$. In an ideal condensation scheme, this should approach unity. Present methods[1,2] seem to require $r \div s > 3$.

Collect $r$ columns of $[D]_p$ *as a subset* $T$, and now define

$$\underset{(n\times 1)}{q} = \underset{(n\times r)}{T} \cdot \underset{(r\times 1)}{\eta}$$

Received January 27, 1972; revision received March 7, 1972.
Index category: Structural Dynamic Analysis.

* Chief, Dynamic Analysis. Member AIAA.

† Chief Engineer, Structural Dynamics. Associate Fellow AIAA.

‡ Engineer, Structural Dynamics.